

*Scientific Report*  
*Regarding the project*  
**“The geomagnetic field under the heliospheric forcing. Determination of the internal structure of the Earth and evaluation of the geophysical hazard produced by solar eruptive phenomena”**

Program IDEI, Contract 93/5.10.2011, Stage I-III, December 15, 2013  
*In the time interval October 2011 – December 2013*  
**(Synthesis)**

### **Introduction**

The proposed research aims at achieving an understanding of the space weather effects on conducting structures inside the Earth and on the surface electric field, with applications to a better knowledge of the internal structure of the Earth at continental (Europe) and country scales, on one hand, and to estimating the geophysical hazard of space weather at midlatitudes, on the other. The main objectives are:

1. To derive the magnetic and electrical properties of the terrestrial lithosphere and mantle at continental and Romanian territory scales;
2. To analyze solar eruptive processes and solar wind components responsible for geomagnetic hazardous activity (geomagnetic storms and substorms) in the time interval 1964-2014;
3. To model the geoelectrical field at the Earth's surface as produced by various magnetospheric and ionospheric current systems;
4. To evaluate the geophysical hazard for technological networks, associated to variations of the geoelectric field during geomagnetic disturbances linked to the interaction of solar coronal mass ejections and high speed streams with the magnetosphere.

The present synthesis shortly describes the main results obtained between October 2011 and November 2013, included in the detailed scientific reports for each of the years 2011, 2012, and 2013. The results refer to:

1. Building the project database;
2. Carrying out systematic geomagnetic measurements at the repeat stations of the National Secular Variation Network and some magneto-telluric soundings in certain areas of interest on the Romanian territory;

3. Modelling the distribution of magnetic and electric properties of the Earth's interior at the scale of the Romanian territory and of the European continent by (a) geomagnetic and (b) magneto-telluric research;
4. Analysis of solar eruptive processes and of the solar wind, responsible for the hazardous geomagnetic activity (geomagnetic storms and substorms).

In the next stage of the project, besides carrying out geomagnetic and magneto-telluric measurements and improving the models obtained so far, the modelling of the surface electric field and its temporal variation under the influence of the hazardous geomagnetic activity, as well as the study of the associated geophysical hazard will be tackled.

## Chapter I. New geomagnetic and magneto-telluric measurements in Romania

**Geomagnetic measurements** have been carried out at the 26 repeat stations that form the so-called National Secular Variation Network, as well as at the Surlari geomagnetic observatory. Several field campaigns covered the time intervals 26.06 – 17.07.2012, 27.08 – 19.09.2012, 24.06 – 06.07.2013 and 11 – 14.07.2013.

The horizontal component  $H$  of the geomagnetic field, the total field  $F$ , the magnetic declination  $D$ , and the geomagnetic inclination  $I$  have been determined by means of a DI-Flux theodolite LEMI 024, two QHM magnetometers, a proton magnetometer Geometrics G-856, and a recording fluxgate magnetometer LEMI 018. The corresponding values were corrected for the diurnal variation and reduced to the moment of the first reading in the series stipulated in the measurement protocols using recordings of the Surlari geomagnetic observatory. Then the values corresponding to the middle of the year were calculated. Having in view the delay of about 1 year for the observatory annual mean to be communicated, in 2012 the values were reduced to the epoch 2010.5 and in 2013 to the geomagnetic epoch 2012.5. These values were used to map the geographical distribution of the geomagnetic elements  $H$ ,  $Z$ ,  $D$ ,  $F$ . As an example, we give in Fig. 1 the distribution for the epoch 2012.5 of the geomagnetic elements based on measurements done in 2013.

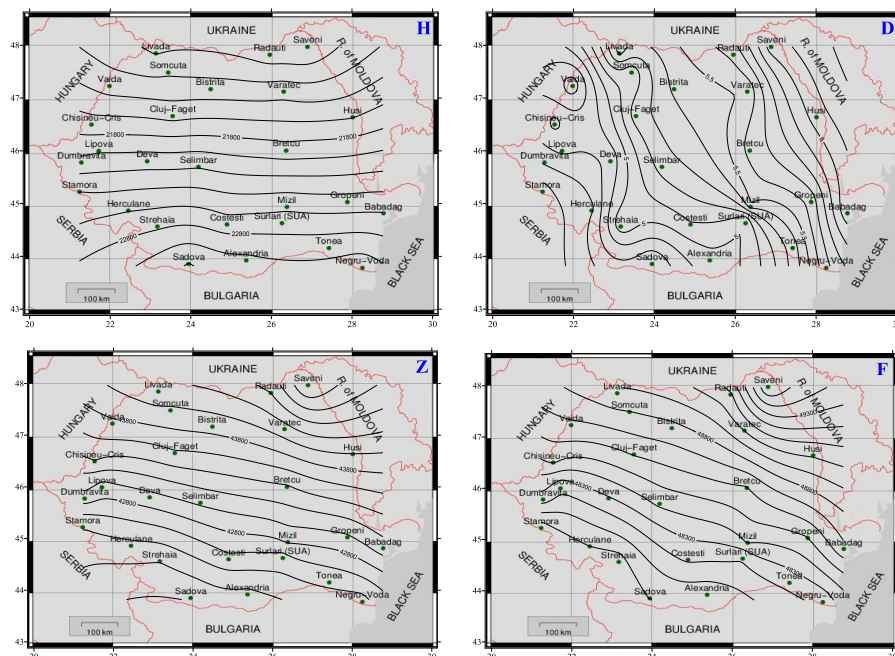


Fig. 1. The geographical distribution (Romanian territory) of geomagnetic elements for the epoch 2012.5 (measurements performed in 2013). The repeat stations and the geomagnetic observatory are marked.

At the 26 stations of the secular variation network, **recording of the field evolution** (the four components, X, Y, Z, F) was performed in parallel with the absolute measurements. The equipment Bartington MAG 03 was tested by means of recordings done in parallel with the ones performed by the LEMI (X, Y, Z) and Geometrics (F) equipment.

**Magneto-telluric measurements** have been carried out experimentally at the Provita de Sus observatory of the Institute of Geodynamics, in 2012, and at Tulnici, in the Vrancea seismogenic area, in 2013. In the scientific report both the measuring method and the obtained results are detailed. In the present synthesis we show the results of a magneto-telluric sounding carried out in Vrancea area, at Tulnici.

Observation data saved in files of the **.ats** type were processed by means of the code package MAPROS. The program computes power spectra using the Fast Fourier Transform, necessary in the determination of the impedance tensor, resistivity and phase curves ( $\rho_{xy}$ ,  $\rho_{yx}$ ,  $\phi_{xy}$ ,  $\phi_{yx}$ ) for a nonrotated and rotated ( $\rho_{\perp}$ ,  $\rho_{\parallel}$ ,  $\phi_{\perp}$ ,  $\phi_{\parallel}$ ) coordinate system. The last ones are known as E-polarized and B-polarized curves (Fig. 2). The complete interpretation of the sounding will be carried out in the next project stage.

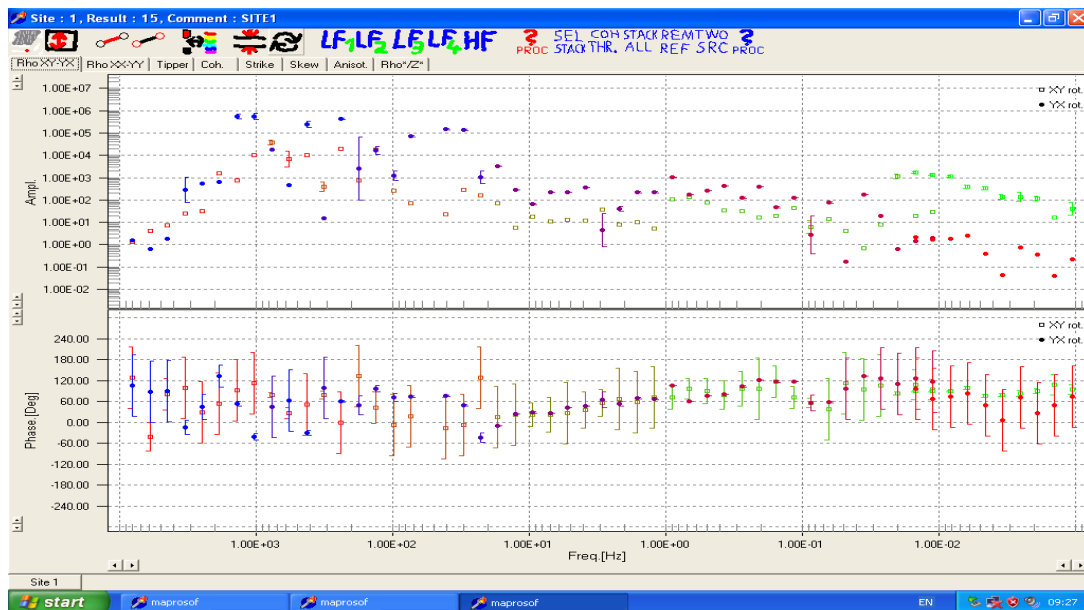


Fig. 2. Resistivity and phase curves ( $\rho_{\perp}$ ,  $\rho_{\parallel}$ ,  $\phi_{\perp}$ ,  $\phi_{\parallel}$ ) for a magneto-telluric sounding at Tulnici, the Vrancea active tectonic region

## **Chapter II. Modelling the distribution of magnetic and electric properties of the Earth's interior at the European and Romanian territory scales based on geomagnetic measurements. The III stage Induction model**

### **2.1. Modelling method**

Usually, the interpretation of data produced by magnetometric networks is based on the assumption that an external variable field induces electric currents in the conductive structures inside the Earth, which in turn produce detectable secondary magnetic fields. The method we used in the present work is based on the observation that the variable external magnetic field induces variable magnetic fields not only by electromagnetic induction, but also by magnetic induction in rocks above the Curie temperature. In case of pure magnetic induction the temporal variation of the field components at a certain observation point is given by the linear combination of the inducing magnetic force (Demetrescu et al., 1985; 1988):

$$\Delta E^{(S)}(t) = \sum_{k=1}^3 C_k^E \Delta F_k(t), \quad (1)$$

where  $\Delta$  represents variations against the temporal average,  $E^{(S)}$  is the field component at the S station (E can be X, Y, Z, or F),  $F_k$ ,  $k = 1...3$  are the inducing force components, and  $C_k^E$  are coefficients depending on the effective magnetic permeability that characterizes the point. The calculated values of the model,  $(\Delta E^{(S)}_{\text{calc}})$ , represents the component of the observed signal produced by pure magnetic induction, and residuals,  $(\Delta E^{(S)}_{\text{res}} = \Delta E^{(S)} - \Delta E^{(S)}_{\text{calc}})$ , contain the information related to the electromagnertic induction in the Earth's interior at the considered point. The coefficients  $C_k^E$  can be determined by a least square procedure and then mapped, resulting images of the lateral (geographical) distribution of the magnetic properties that characterize the rock volume above the Curie temperature (generally the crust). To ensure the comparability of coefficients corresponding to various stations, recordings should be simultaneous in all stations, in order to study the same time interval proper to the inducing external force. Consequently, the mentioned temporal averages refer to the common recording interval.

Up to now, the method had been succesfully applied in case of the national repeat station network (Demetrescu et al., 1985) and in case of the European network of geomagnetic observatories (Demetrescu et al., 1988; Demetrescu and Andreescu, 1992, 1994; Demetrescu and Dobrică, 2003), for the 11-year solar cycle signal, as well as in case of the Hokkaido (Japan) magnetometric network (Dobrică et al., 2008-2009), for the diurnal variation.

In the Research Report for the Stage II of the contract (the year 2012), results concerning the **magnetic properties** of the crust obtained by applying the method are described, both in case of the Romanian territory and in case of the observatory network at the European scale. The methodology, described in detail in that Report was slightly different in the two cases, because the simultaneity of observations in all network nodes was possible only in case of the European observatories. To use the recordings acquired in the national network of repeat stations in a time-span of several hours, but in different days, some changes in the methodology were necessary. The information offered by the horizontal component of the geomagnetic field was used in case of the European network, but all the field components in case of the Romanian network. The model of the lateral distribution of the magnetic properties of lithosphere, obtained in the 2nd stage of the project (2012) is presented in Fig. 3, for the Romanian territory, and in Fig. 4 for the European territory covered by the INTERMAGNET observatories network.

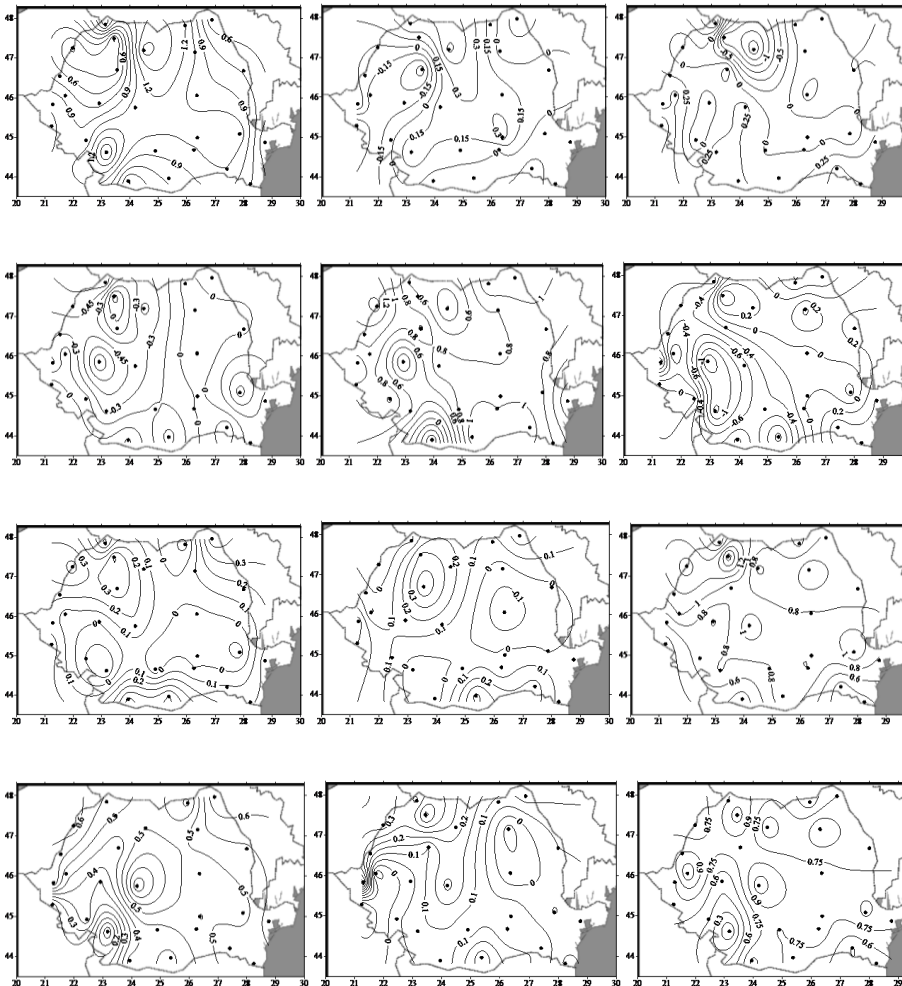


Fig. 3. Model of the lateral distribution of the lithosphere magnetic properties on the Romanian territory, corresponding, from top to bottom, to: the North horizontal component, X, East horizontal component, Y, vertical component, Z, and the total field, F. From left to right, the coefficients C1, C2 și C3 of eq. (1)

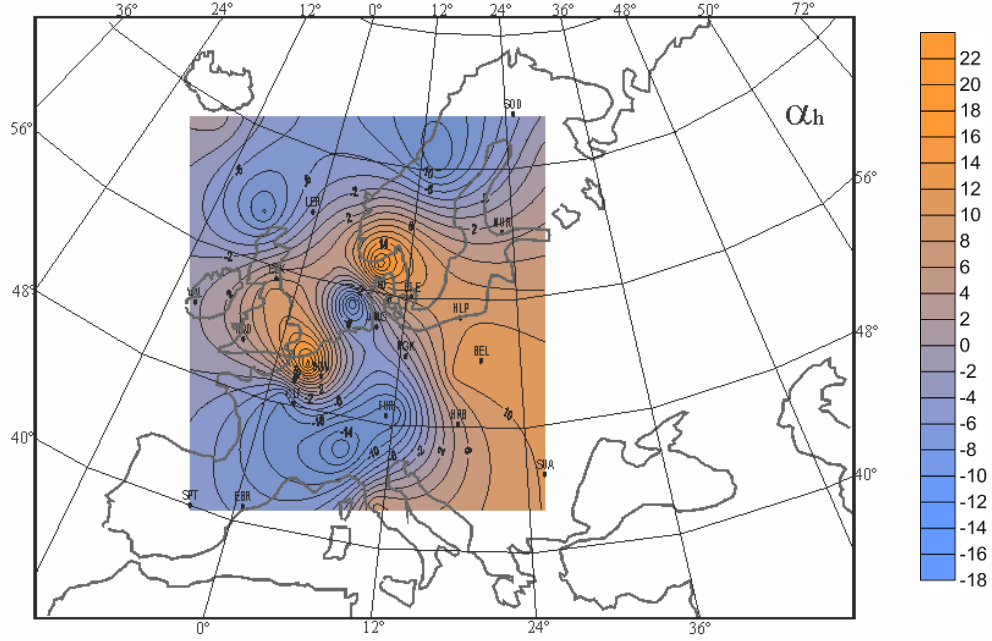


Fig. 4. Model of the lateral distribution of the lithosphere magnetic properties in Central and Western Europe

In case of the **electric properties** of crust and mantle, the residual of the Induction Model for the **vertical component** of the field is used. The latter responds to a larger extent to the induction in the electrically conducting structures than does the horizontal component. As the induction electromotive force is given by the negative time derivative of the inducing magnetic flux, the latter should correlate with the observed residual. In terms of loops of current that flow in the more conductive layers of the Earth's interior, having in view the proportionality between the magnetic field of intensity  $B$  produced by the current of intensity  $I$  in the loop

$$B = 2\pi k \frac{I}{a}$$

where  $k = 10^{-7} \text{ WbA}^{-1}\text{m}^{-1}$ , and  $a$  is the loop radius, the residuals can be viewed as a measure of the current intensity in an equivalent circular loop of radius unity around the observation point. This allows estimating the inductance  $L$  and the resistance  $R$  of the equivalent circuit, based on the well known relationship between the instantaneous value of the tension,  $u$ , and of intensity,  $i$ , in an R-L circuit (circuit with inductance).

$$u = L \frac{di}{dt} + Ri$$

Tension is equivalent with the negative time derivative of the inducing vertical magnetic field, and the current intensity with the residual of the Induction Model for the vertical component. With these equivalences the following relationship is obtained:

$$-\dot{Z}_{sursa}(t) = L \cdot \dot{Z}_{rez}(t) + R \cdot Z_{rez}(t)$$

where  $\dot{Z}_{sursa}(t)$  is the temporal derivative of the vertical component of the field produced by the inducing source, and  $Z_{rez}$  is the residual of the induction model applied to the vertical component  $Z$  recorded at the observation site.  $L$  and  $R$  can be determined for each observatory, for the given time interval, by means of the least squares method. Mapping the obtained values gives the lateral distribution of the electric properties of the interior. The mapped values are relative ones, the corresponding maps reflecting, as was the case of magnetic properties (the 2012 Report), the lateral variation of the parameters  $L$  and  $R$ , not real (absolute values) inductances and/or resistances. Also, the obtained information describes properties regarding a large depth range, from surface to mantle depths.

## 2.2. Data

**For the Romanian territory** measurements performed in 2010 in the National Secular Variation Network were used. As a proxy for the external sources recordings of Surlari geomagnetic observatory, located within the network, and from the Niemegek observatory, at about 1000 km from the network. Measurements were carried out in four campaigns: 17.06-7.07, 30.07-18.08, 14.09-22.09 și 1.10-14.10.2010. In each station 7-8 hours-long recordings were obtained for the components X, Y, and Z, generally between 8 and 17 standard local time (SLT) (5-14 UT), by means of the magnetic variometer LEMI-18. In parallel recordings of the total field, F, were obtained by means of a proton magnetometer Geometrics G-856. One-minute recorded data were used. To model the electric properties the vertical component Z data was used.

**For the European continent** one-minute values for a subset of observatories, namely the INTERMAGNET ones (19 observatories), with data at [www.intermagnet.org](http://www.intermagnet.org). The external source was represented by the variations of the magnetospheric ring current during the major geomagnetic storm of May 15, 2005, through the one-minute Dst geomagnetic index available at <http://geomag.usgs.gov/data>. That index represents the effect of the ring current at the Earth's surface in the geomagnetic equatorial area.

### 2.3. Results

For each station/observatory the coefficients of eq. (1), the calculated values of the model, and the residuals were computed. The calculated values of the model were used to map the lateral distribution of lithosphere magnetic properties, discussed above (Fig. 3 and 4). We remind (see the scientific report for 2012) that in case of the European network the effect of the ring current was calculated for each observatory by means of the relationships:

$$\Delta Z_s^{H_s}(t) = \frac{\alpha_h}{\beta_h} \Delta H e(t) + \frac{\alpha_z}{\beta_z} \Delta Z e(t)$$

$$H e = \frac{M}{r^3} \cos \varphi = Dst \cdot \cos \varphi$$

$$Z e = \frac{2M}{r^3} \sin \varphi = 2Dst \cdot \sin \varphi$$

in which  $\theta$  is the colatitude of the observing point.

The model residuals, together with the time derivative of the recorded vertical component, were used to derive the parameters L and R, **the inductance** and **the resistance**, for each observation point. Mapping those values produced images shown in Figs. 5 and 6.

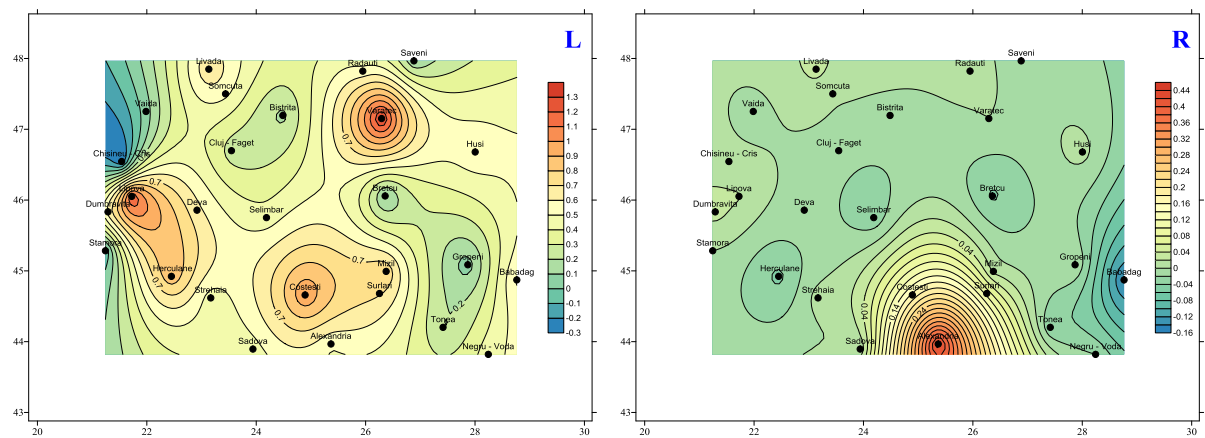


Fig. 5. The lateral distribution of the magnetic inductance (left) and electric resistance (right) of the crust and upper mantle in Romania

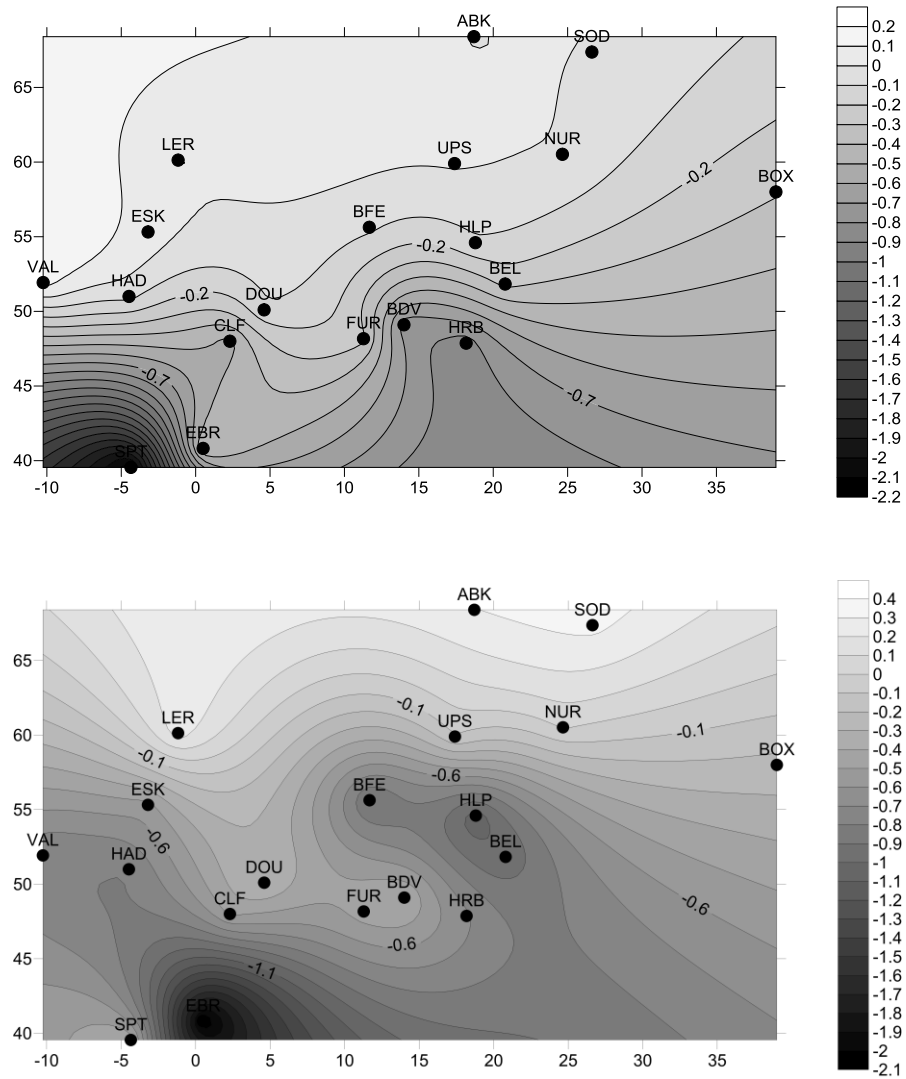


Fig. 6. The lateral distribution of electric properties of crust and upper mantle in Central and Western Europe. Top – the magnetic inductance, bottom – the electric resistance. Symbols indicate INTERMAGNET observatories

The information obtained in this stage will be used in the next stages of the contract, to determine variations of the electric field and surface currents that form during hazardous major geomagnetic disturbances.

## **Chapter III. Model for electric properties of lithosphere on the Romanian territory, based on magneto-telluric measurements, Stage III**

The magneto-telluric method (MT) is sensitive to detection of interconnections due to partial melts, fluids, and graphite inclusions. In tectonic active areas, reduced percentage of partial melts and saline fluids form conductive structures distinct from the surrounding environment, while in stable areas, old tectonic processes can be found as conductive zones as a result of collisions between various crustal units.

Magneto-telluric measurements (MT soundings) organized on profiles lead, by their interpretation by dedicated methods of inversion, to obtaining useful information on the lateral and depth distribution of electric properties of lithospheric rocks. Within the frame of the present contract 2D crustal and lithospheric models along representative cross-sections regarding the electric resistivity of various tectonic units and geological formations, presented in detail for the stages II (2012) and III (2013) of the contract. In the present synthesis we show three such cross-sections, as well as a map of the lateral variation of the electrical conductance associated to the Carpathian chain and foredeep, based on detailed magneto-telluric soundings in those areas. In Fig.7 the cross-sections discussed in the next section of the report are presented.

### **3.1. 2D resistivity models – representative geotraverses**

#### **3.1.1. Method**

To build cross-sections and 2D models the existing magneto-telluric data bank was used, as well as the information obtained from two magneto-telluric soundings. Observation data saved in **.ats** files were processed by means of MAPROS package. This program computes power spectra by Fast Fourier Transform, necessary to calculate the impedance tensor, and the resistivity and phase curves ( $\rho_{\perp}$ ,  $\rho_{\parallel}$ ,  $\varphi_{\perp}$ ,  $\varphi_{\parallel}$ ), also known as E-polarized and B-polarized curves.

The interpretation of resistivity curves implies two stages: solving the inverse problem, which offers an almost qualitative image of the depth distribution of the resistivity, and solving the direct problem, that implies obtaining the quantitative model showing the vertical extension of structures and associated resistivities.

The inversion algorithms are applied based on simplifying working hypotheses that approximate the real geological conditions. For this report, to solve the inverse problem the Marquard and Niblett–Bostick procedures were applied. The analytical solutions for complex 2D structures were obtained by means of numerical methods, using techniques based on

solving differential equations, that lead to analysis of a set of algebraic linear equations. The computer program simulates magneto-telluric responses for E-polarized and B-polarized cases using the finite element technique. The results would be representative for the geoelectric characterization of the investigated structures due both to its resolution and conditions in the limit imposed by the program.

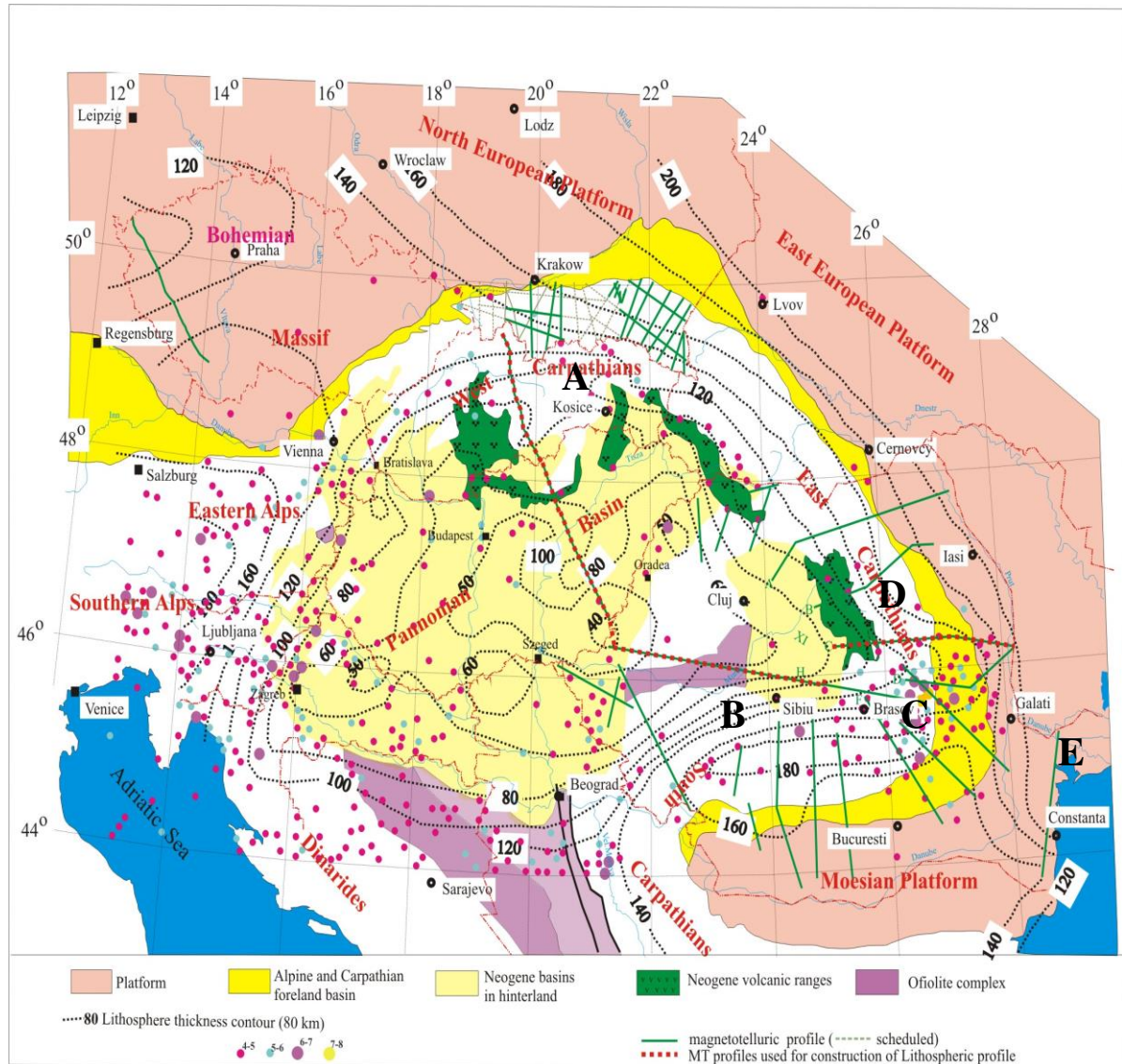


Fig. 7. Location of magneto-telluric cross-sections in major structures in Romania (**B**, **C**, **D** and **E**), Slovak Republic and Hungary (**A**) – full circles. Green geotraverses (full lines) have been used to infer the distribution of the electric conductance on the Romanian territory.

### 3.1.2. Main results

#### *2D model, geotraverse D (Bistrița-Vatra Dornei- Suceava)*

The final result of the 2D modelling on the geotraverse D of Fig. 7, presented in Fig. 8, reflects the depth structure at crustal level based on resistivity values. The model was obtained after 11 iterations by means of the finite element program. It represents the closest image to the real one, as between calculated response functions and experimental values

there is a maximum difference of only 5%. According to figure legend, the model displays resistivities of 5-3,000  $\Omega\text{m}$ , distributed to a depth of more than 40 km.

The resistivity values show that the Trans-European Suture Zone (TESZ), also known as the high electric conductivity zone (ACEC), develops along the consumption paleoplane of primary basement of the Carpathian fish nappes. In the 2D model the following important characteristics are found: width of 7-8 km, vertical development between 10 and 40 km, 10  $\Omega\text{m}$  resistivity.

The sedimentary cover of the Transylvanian Basin and of the Carpathian foredeep show resistivities of 5  $\Omega\text{m}$  and respectively 10-50  $\Omega\text{m}$ . The Central East Carpathian nappes show values between 100 and 300  $\Omega\text{m}$ , while the Precambrian metamorphosed socle of the East European Platform is characterized by resistivity values between 500 and 1000  $\Omega\text{m}$ .

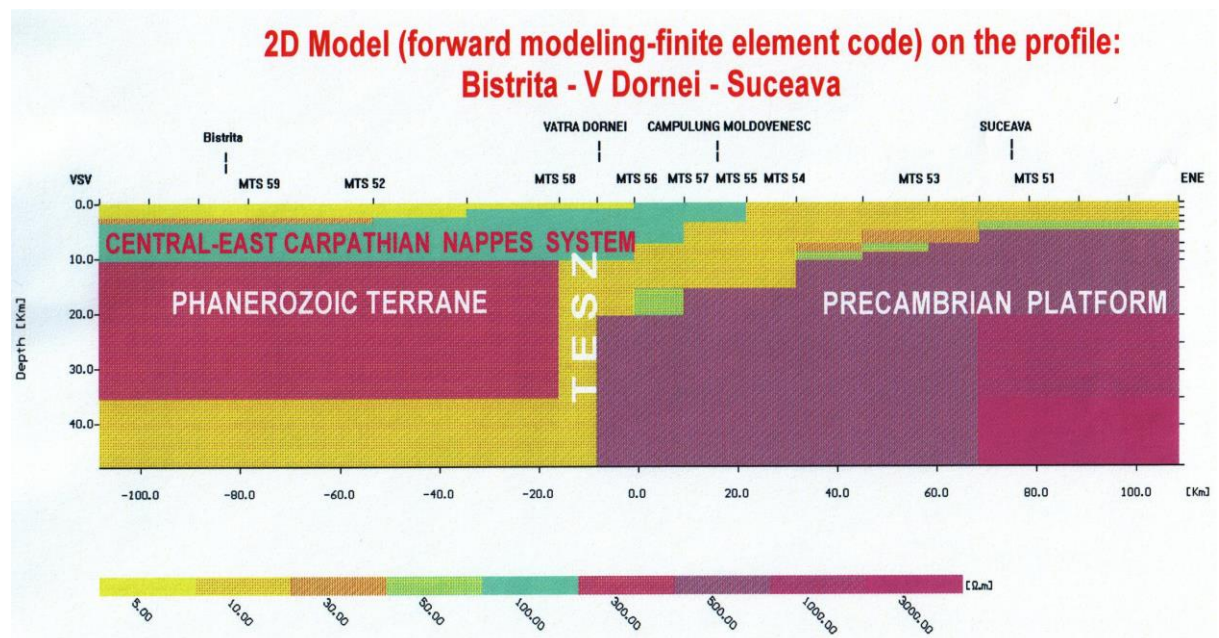


Fig.8. 2D Model of resistivity distribution along the D geotraverse Bistrița- Vatra Dornei- Câmpulung Moldovenesc-Suceava ; MTS 59 – magneto-telluric sounding

***2D Model along the geotraverses A, B and C crossing Slovak Republic, Hungary and Romania***

The results for geotraverses A, B, C of Fig. 7 are presented in Fig. 9 (the segment B) and in Fig. 10 (segment A and C).

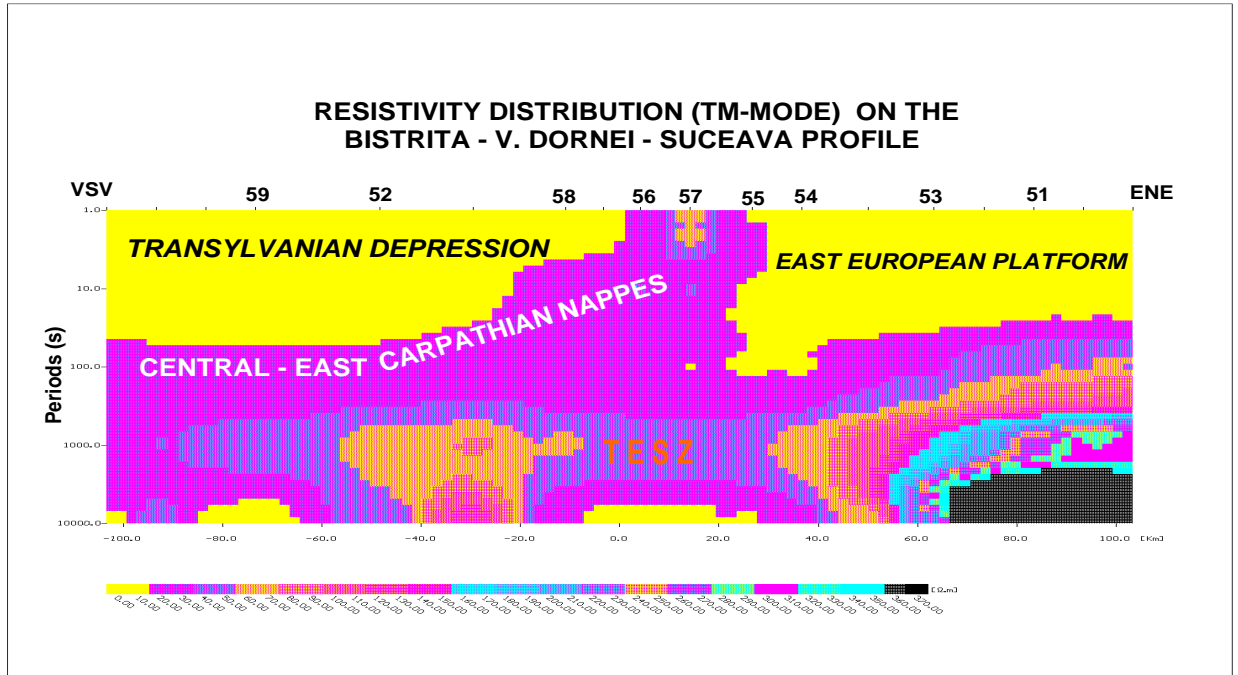


Fig. 9. 2D Model for the Pannono-Carpathian geotraverse (segment B)

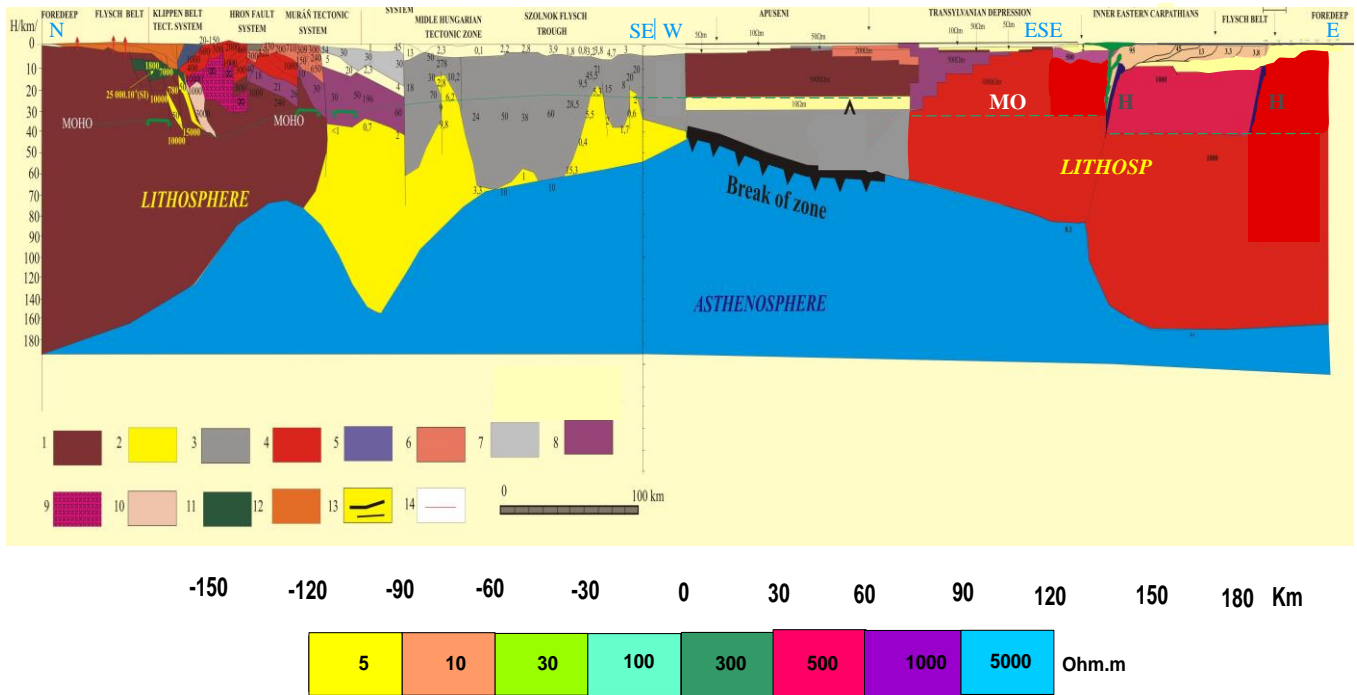


Fig. 10. 2D tomography along the Pannono-Carpathian geotraverse (segments A, B, C)

The aspect of resistivity isolines suggests the existence of several structures as follows:

- The Major Tethian Suture (red) (culoare roșie) associated with a mean resistivity of 500  $\Omega\text{m}$ ;
- The Paleogene-Neogene post-tectogenetic sedimentary cover in the Pannonian Depression, with resistivities ( $\rho$ ) between 5-30  $\Omega\text{m}$ ;
- The Neogene and Paleogene-Mesozoic post-tectogenetic sedimentary cover in the Transylvanian Basin with  $\rho = 5-30 \Omega\text{m}$ ;
- The nappe system Biharia-Căpâlnaș-Techereu is represented by  $\rho = 300 \Omega\text{m}$ ;
- The Bihor Unit has  $\rho = 1000 \Omega\text{m}$ ;
- The Central-East Carpathian nappes and their metamorphosed basement are represented by high resistivity values ( $\rho = 1000 \Omega\text{m}$ );
- At the base of the Bihor unit (base of the Pannonian crust – Apuseni Mts.) a brittle/ductile transition zone with  $\rho = 10 \Omega\text{m}$  is present;
- The lithosphere/asthenosphere boundary, at 60 km depth (Vărșand – Pannonian Depression) and at 85 km depth (Hoghiz – Transylvanian Depression), is characterized by a low resistivity, due probably to the presence of partial melts.

Additionally, we mention:

#### For the segment A

- The existence of a lithosphere with variable thickness (90-180 km) on the north-western segment and a thin one (45-60 km) under the Pannonian Depression;
- The presence of a conducting layer (2-10  $\Omega\text{m}$ ) at the crustal base on the Pannonian Depression segment;
- The presence of two conducting zones (50  $\Omega\text{m}$ ), developed almost vertically in the rooting zone of Carpathian nappes;

#### For the segment C

- In the area of the Scitian and East European Platforms the lithosphere is approximately 180 km thick;
- The presence of two high conducting zones (HCZ) that correspond to the Trans European Suture Zone and, respectively, to the Carpathian Conductivity Anomaly (ACEC);
- A platform cover with resistivities of 2-10  $\Omega\text{m}$ .

### **3.2. The distribution of electric conductance over the Romanian territory**

The conductance (the inverse of the electric resistance referred to the formation thickness) can be derived by means of:

$$S = 796 \left[ \frac{1}{Z} - \sqrt{\frac{T}{10\rho}} \right],$$

where: S is conductance [ $\Omega^{-1}$ ], Z is the magneto-telluric impedance [mV/km], T is the period [sec], and  $\rho$  is the resistivity.

Using all magneto-telluric soundings on profiles marked with green lines in Fig. 7 that cross the South and East Carpathians as well as the foredeep and platform structures in front of them, a map of the conductance has been constructed, shown in Fig. 11. Low values of conductance ( $S < 100 \Omega^{-1}$ ) characterize the crystalline-mesozoic area of the East Carpathians and the Getic and Supragetic nappes of the South Carpathians, and values higher than  $1100 \Omega^{-1}$  are associated to the sedimentary formations of the foredeep. The sedimentary cover of the East European Platform and Moesian Platform is characterized by values of  $300-500 \Omega^{-1}$  and, respectively,  $600-900 \Omega^{-1}$ .

The results presented in this section underline the high degree of inhomogeneity of the crust and upper mantle from the view point of the electric conductivity. The increased conductivities are caused by the presence of graphite, sulfurs, partial melt fluids, high temperature etc. Also, it is seen that the Trans European Suture is a major conducting electrical boundary that divides the Paleozoic Europe of thin lithosphere (45-150 km) from the East European Craton of thicker lithosphere (cca 200 km). The lithospheric thickness as indicated by the MT soundings are marked in Fig. 7.

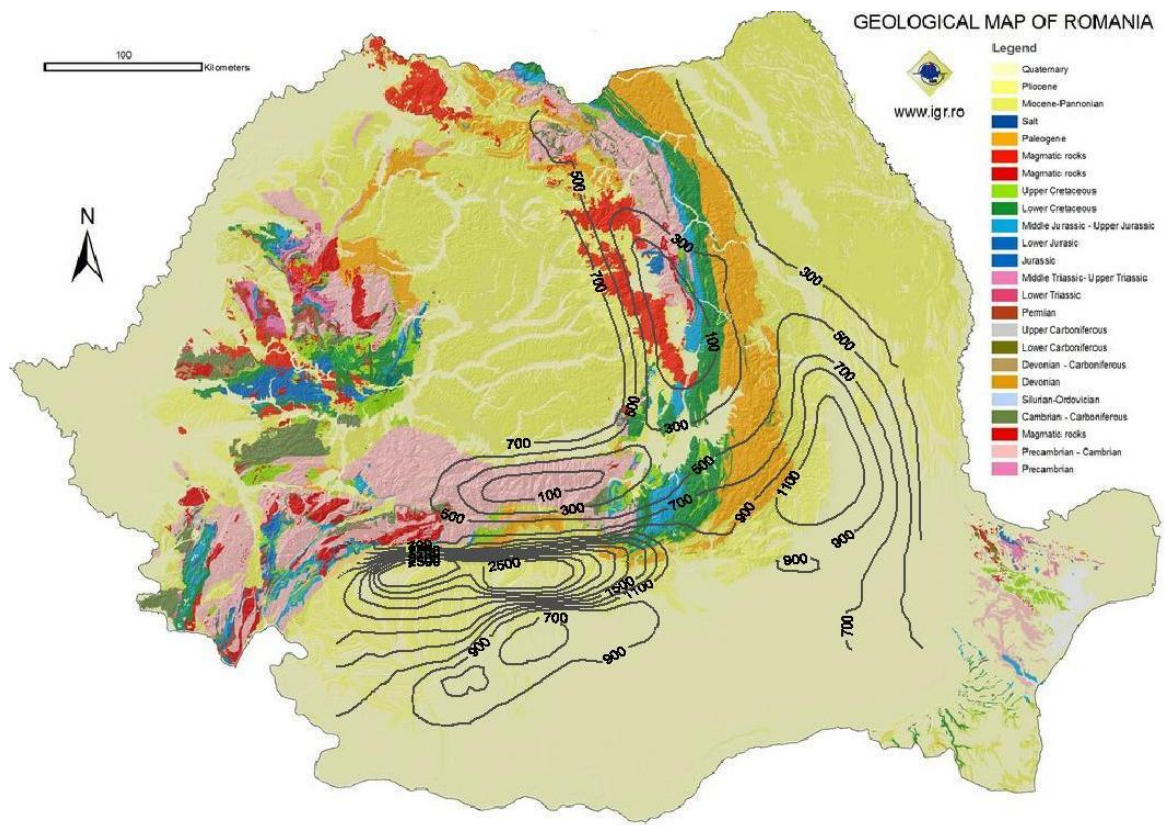


Fig.11. The map of conductance distribution on the Romanian territory (black lines)

## Chapter IV. Analysis of some solar eruptive processes and of the solar wind from the viewpoint of their geoeffectiveness

### 4.1. The sources of midlatitude geomagnetic activity

The terrestrial magnetic field, produced by a dynamo process in the outer core of the Earth, extends in space, becoming basically a dipolar field. Under the solar wind action the magnetosphere extends to distances of the order of 100 Earth radii and gets a specific „aerodynamic” shape. As the result of the interaction of the solar wind and the heliospheric (or interplanetary) magnetic field with the magnetosphere, in the latter and in the ionosphere current systems form that produce, in certain conditions, disturbances of the geomagnetic field of the geomagnetic storm or substorm type. These could present hazardous effects for technological systems (electric power systems, hydrocarbon pipes), on one hand, and for the human health, on the other. The main current systems are monitored by means of the so-called geomagnetic indices: the magnetospheric ring current evolving at a distance of 5-7 Earth radii by means of the **Dst** index, the auroral electrojet evolving in the subpolar ionosphere at heights of 100-150 km by means of **AE**-type indices (AU, AL, AE), and the geomagnetic activity at middle latitudes, as cumulated effects, by means of the **aa** index. Geomagnetic indices are calculated and maintained within the frame of several World Data Centers, based on recordings provided by geomagnetic observatory networks properly located on the Earth’s surface. The aa index is derived using records from two antipodal observatories, Hartland, in England, and Canberra, in Australia.

In the 2012 stage of the present contract a special attention has been given to long-term evolution of magnetosphere and current systems developing in the magnetosphere and ionosphere under the impact and by interaction with coronal mass ejections (CMEs) and high speed streams (HSS) in the solar wind. Along this line of research, both the correlation between various current systems and the temporal evolution of the interplanetary geoeffective electric field  $E_m$ , illustrated by means of the PC index, recently introduced (1980). Based on that study, we succeeded to reconstruct back to 1868 both of the PC index, so indirectly the interplanetary geoeffective electric field, and the magnetospheric ring current and the ionospheric auroral electrojet. and were presented. In Fig. 12 we show, as an example, the PC index evolution from 1868 on, based on the observed correlation between various geomagnetic indices and solar wind and heliospheric magnetic field parameters measured during the space era (since 1964).

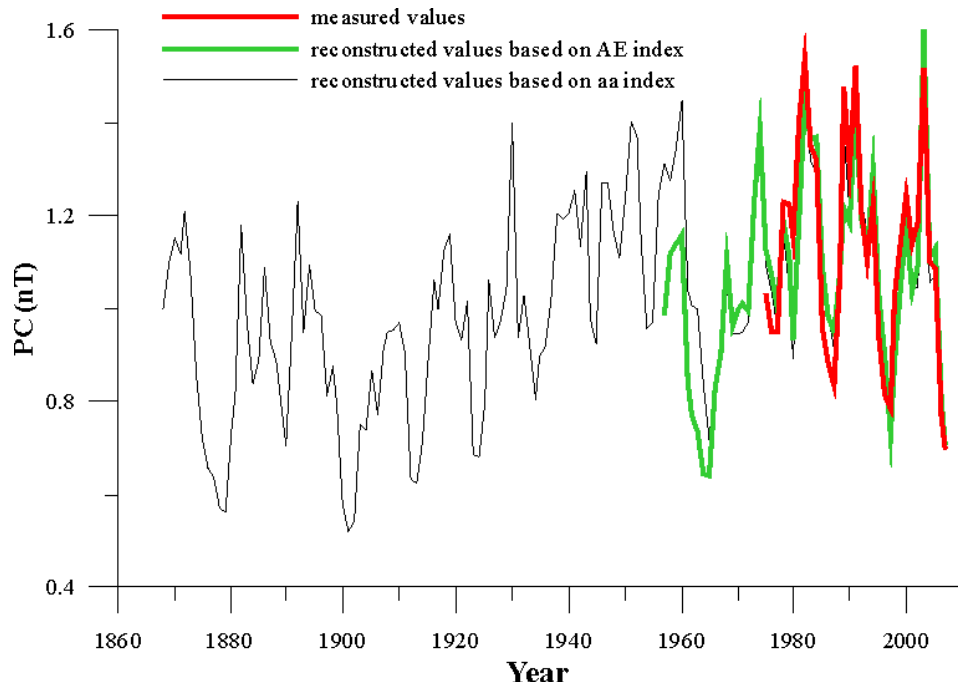


Fig. 12. Reconstruction of PC index (observed value – red) based on AE (green ) and aa (black)

In the 2013 stage, in order to characterize in a larger detail the geoeffectivity of solar processes and of the solar wind, a study on causes producing geomagnetic activity at middle latitudes have been carried out, analyzing the contribution of the magnetospheric ring current and of the ionospheric auroral electrojet to the geomagnetic field variations recorded in the network of European geomagnetic observatories. The steps in processing data are illustrated in Fig. 13, for the case of the Niemegek (NGK) observatory (Germany). Data of the northern horizontal component of the field,  $X$ , have been corrected for the quiet solar diurnal variation,  $S_q$ , resulting in the disturbance variation,  $S_D$ .

$S_q$  is produced by the so-called ionospheric dynamo, is controlled by the ionization in the upper atmosphere (ionosphere) due to ultraviolet solar radiation, and was determined from the variation recorded in the five most calm days of the month. Next, the  $S_D$  variation was modelled by means of the Dst index, and the residual by means of the AE index, used as proxies of the two current systems, the magnetospheric ring current and the ionospheric auroral electrojet. In the detailed scientific report for the year 2013 the results obtained in the successive steps and at end. For the 26 observatories, modelling by means of Dst and AE geomagnetic indices resulted in the reduction of the mean square variation of  $S_D$  to 0.1-2.9 nT, from 8-48 nT (Fig. 14). The histograms in the figure are ordered according to the increasing latitude of observatories as listed in the corresponding table in the detailed scientific report. The global reduction for the 26 observatories is from 16.3 nT to 1.2 nT, i.e. of 93%, demonstrating that the recorded geomagnetic activity at midlatitudes is entirely produced by the two current systems.

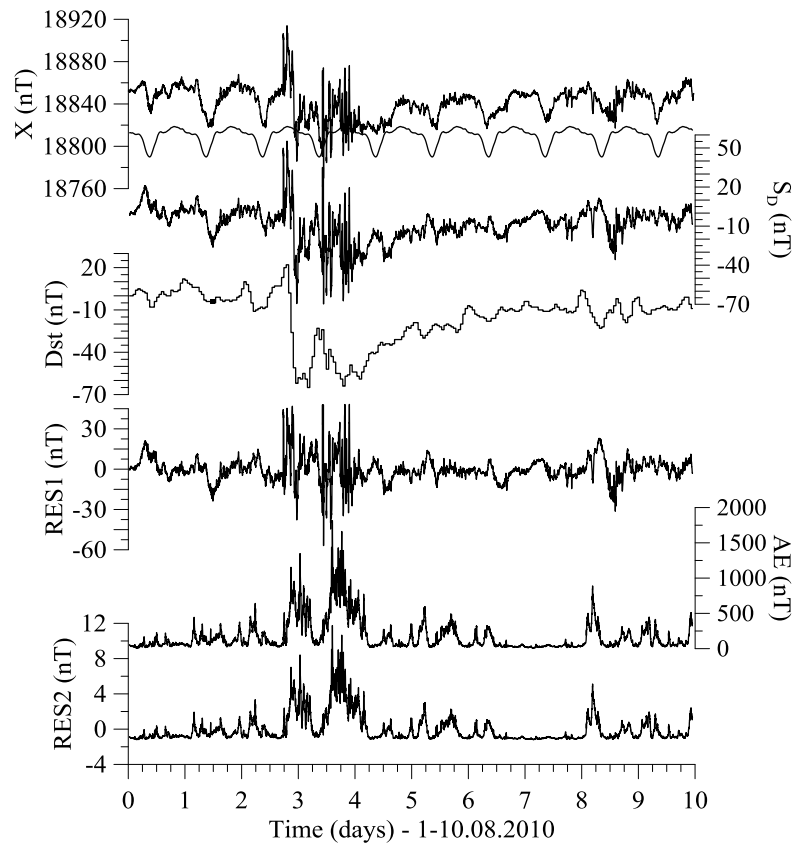


Fig. 13. The steps of processing recorded geomagnetic data at NGK. From top to bottom, X,  $S_q$ ,  $S_D$ , Dst, RES1, AE, RES2

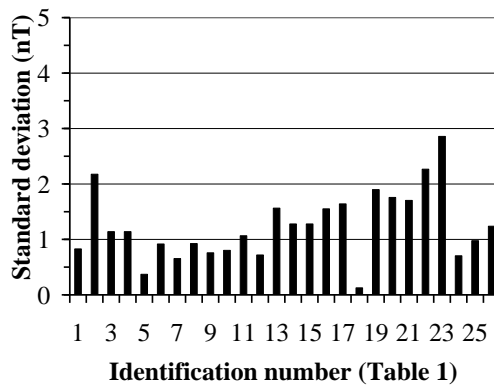
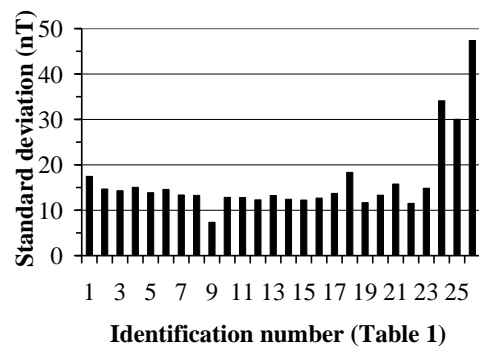


Fig. 14. Top – the mean square error of  $S_D$  for INTERMAGNET European observatories.  
Bottom – the mean square error of the residual disturbance

## 4.2 Geoeffectiveness of certain solar events

The geoeffectiveness of solar phenomena depends on two essential factors: their energy and the propagation direction from the Sun to Earth. The energy of certain eruptive phenomena is directly dependent of the solar source, its position with respect to solar atmospheric layers, the magnetic structure in the source, the solar particles (plasma) ejection speed. The propagation direction is influenced by the position of the source phenomenon on the solar disk (the events generated in the western hemisphere have a greater probability of reaching Earth considering the spiral-like structure of the solar wind) and by the particles flux extension during the propagation (the most efficient CMEs are the Halo-type ones or those with an angular width greater than  $120^\circ$ ). In solar maximum activity periods there are often eruptive events succeeding at intervals of a few hours (CMEs or solar flares that appear in the same active region), or events that appear at small time intervals from different sources and interact during their propagation in space (CME and HSS); the geoeffectiveness of such a complex event may significantly increase or decrease, as a function of the magnetic structure of the plasma that leaves from the solar sources and interact during their propagation. The most important role in geoeffectiveness is played by the  $B_z$  component of the interplanetary magnetic field: the negative  $B_z$  (southward oriented) allows the reconnection between the heliospheric and the terrestrial field. No matter how “energetic” an eruptive phenomenon may be, if  $B_z$  is positive when the solar plasma arrives at the magnetosphere boundary, the reconnection is not produced and the plasma flux avoids the terrestrial magnetosphere undergoing a secondary reconnection in the magnetospheric tail. Solar particles that thus enter the magnetosphere, propagate towards the auroral ovals producing the polar auroras and often magnetospheric perturbations of small intensities and short duration (geomagnetic sub-storms).

The study undergone for the solar cycle 23 maximum concerning major geomagnetic storms (superstorms,  $Dst \leq -200$ , 9 events, Table 4.2.1, and intense geomagnetic storms,  $Dst \leq -100$ , 34 events) has shown the following observations concerning the geoeffectiveness of the solar eruptive phenomena (CIR – corotating interaction regions, CME/ICME – coronal mass ejections, flares):

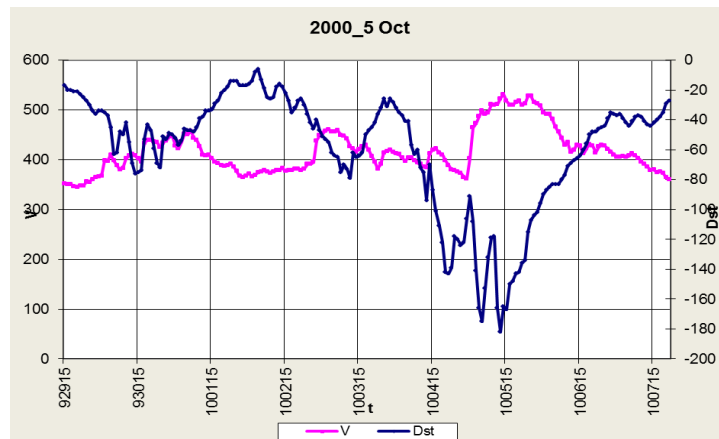
Tabelul 4.2.1. Major geomagnetic storms recorded in the maximum phase of the solar cycle 23

	Year	Date mm/dd/hh	$Dst_m$ (nT)	$Bz_m/\Delta t$ (nT/h)	Solar/Heliospheric sources			$W_\epsilon$ [J]
					CIR	Flare	CME/ICME	
1	1999	10/22/06	-237	-30.7/-1	CH <sup>2</sup> /CIR <sup>1</sup>	-	CME/ICME-CIR <sup>3</sup>	$1.747 \times 10^{17}$
2	2000	04/06/22	-287	-27.3/-1	-	F <sup>2</sup> /C9.7	CME/ICME <sup>3</sup>	$1.667 \times 10^{17}$

3	2000	07/16/00	-301	-49.4/-4	–	F <sup>2</sup> /X5.7	CME/MC <sup>3</sup>	9.952×10 <sup>17</sup>
4	2000	08/12/09	-235	-29.7/-1	–	F <sup>2</sup> /C2.3	CME/MC <sup>3</sup>	2.091×10 <sup>17</sup>
5	2000	09/17/23	-201	-23.9/-2	–	F <sup>2</sup> /M5.9	CME/ICME <sup>3</sup>	9.248×10 <sup>16</sup>
6	2001	03/31/08	-387	-44.7/-2	–	F <sup>2</sup> /X1.7	CME/ICME <sup>3</sup>	2.762×10 <sup>17</sup>
7	2001	04/11/23	-271	-20.5/0	–	F <sup>2</sup> /X2.3	CME/MC <sup>3</sup>	2.868×10 <sup>17</sup>
8	2001	11/06/06	-292	-64.0/-3	–	F <sup>2</sup> /X1.0	CME/ICME <sup>3</sup>	–
9	2001	11/24/16	-221	-27.8/-5	–	F <sup>2</sup> /M9.9	CME/ICME <sup>3</sup>	3.411×10 <sup>17</sup>

(1 – Cid, C. et al, 2004; 2 – Maris O., Maris G., 2009; 3 – Zang, J. et al, 2007).

- The combination of complex sources (CIR and ICME or flares and CME) induces significant negative values of Dst and they maintain these values for several hours;
- The energy input in the magnetosphere, evaluated by the Akasofu parameter (last column) is proportional to the plasma speed, but also to the heliospheric field intensity, and the duration of the reconnection depends on the time interval when Bz remains negative;
- The solar eruptive phenomena that come from different sources, with different magnetic structures, determines the complex structure of the principal phase of the geomagnetic storms, such as illustrated by Fig. 15.



No	Date mm/dd/hh	Dst min (nT)	Bz min (nT)/Δt <sub>min</sub>	Δt (h) (Bz<0)	SSC	Solar/Heliospheric sources		
						CIR	Flare	CME/ICME
11	10/05/13	-182	-17.5/-2h	3 h	SSC	CIR <sup>1</sup>	Flare <sup>2</sup> / ?	CME/ICME <sup>3</sup>

Fig. 15. Geomagnetic storm from October 5, 2000: top frame represents the solar plasma speed variation (V) and the Dst index; bottom frame shows the data characteristic for the geomagnetic storm

### **4.3. Solar wind high speed streams (HSSs) geoeffectiveness. Empirical modelling of geomagnetic storms produced by HSS in the solar cycle 23.**

The empirical modelling of a particular phenomenon implies the setting of some existing relationships between certain experimental data types of the analysed phenomenon. Because of this it is necessary that the data be chosen to be relevant for the analysed phenomenon, for those referring to the statistical evaluation of the phenomenon behaviour as well as for those referring to its physical nature, where this is possible. The term “data” firstly implies choosing the appropriate parameters, then setting some measurements series in time such that the length of the series be relevant to the variability (periodicity) of the phenomenon.

Empirical models can be used to establish some mathematical relationships for giving prognosis for certain phenomenon and for underlying tendencies of the parameter series used. Subsequent series (or even older ones but such that they have not been used for empirical modelling) can be used for testing these models.

In the present study, we focus on studying the high speed streams in the solar wind (HSS) produced by coronal holes and the geomagnetic storms (GS) produced by the impact of the HSS on the terrestrial magnetosphere. We used data concerning HSS that are found in the HSS Catalogue (Maris & Maris, 2012) for the solar cycle 23, 1996 – 2008 (SC 23). We did not take into consideration the HSSs that have interacted with some other fluxes of solar particles (produced by flares or coronal mass ejections) during their propagation or those that have superimposed on some sectorial boundary of the interplanetary magnetic field.

We considered for this study the geomagnetic storms of moderate intensity ( $-100 \leq \text{Dst} \leq -50$ ) and the intense storms ( $\text{Dst} \leq -100$ ). For the storms we used the Complex Catalogue HSS\_GS (Maris & Maris, 2010). Some data (Dst and Bz values) were updated from the final values of the parameters using the OMNI database (<http://omniweb.gsfc.nasa.gov/>).

Table 4.3.1 contains the data used about: HSS, magnetic polarity dominant of the sector in the interplanetary space (IMF) on the duration of the HSS and the data about GS (we present hereunder as an example, an excerpt from the beginning of the table; the entire table can be found in Appendix 1). Columns 1 – 3 refer to the data from the beginning of the HSS (recorded by the ACE mission), columns 4 – 7 show HSS parameters ( $V_0$  – initial speed,  $V_{\max}$  – maximum velocity, duration and  $\text{DVM} = V_{\max} - V_0$ ). The eighth column shows the IMF polarity. Columns 9 – 13 show: the minimum value of the negative Bz recorded before the beginning of the storm,  $\text{Dst}_{\min}$  = the minimum value of the Dst, the day of the Dst minimum value recording (month; day; hour), information about the beginning of

the storm (SSC – sudden storm commencement), GS – gradual storm, dt/t, Bz<0 – the interval from the minimum Bz and the minimum Dst / the number of hours that Bz remained negative.

Table 4.3.1. List of high speed currents produced by coronal holes that have triggered geomagnetic storms

An	Lună	Zi	V0	VMax	Durată	DVM	IMF	Bz min	Dst_min	t-Dst	Tipul furtunii	dt/t, Bz<0
			km/s	km/s	zile	km/s		nT	nT	ll:zz:hh		
Curenți de mare viteză în vântul solar (HSS)							Furtuna geomagnetică (FG)					
1996	3	9	320.3	571.7	7.2	251.4	-	-8.3	-60	3:11:03	GS	-2h/12h
1996	3	19	379.7	643.7	5	264	-	-5.2	-54	3:20:23	GS	-2h/21h
1996	3	24	423	577.7	3.9	154.7	-	-7.2	-60	3:25:01	GS	-2h/9h

The high speed solar wind streams that have produced geomagnetic storms are not uniformly distributed during the solar cycle (second row in Table 4.3.2). The solar source of the HSS are the coronal holes (CH), regions of divergent coronal magnetic field, distributed throughout the entire solar corona thus: at maximum solar activity they are limited to polar regions, over 60° latitude, at minimum solar activity they extend through medium latitudes, sometimes close to the equator vicinity. The solar particles propagation from the coronal holes follow a spiral-like path due to the solar differential rotation. The most efficient solar particles in perturbing the terrestrial magnetic field are those emitted near the ecliptic, close to the solar equator. This means that at minimum activity, HSS can produce more geomagnetic storms (1996).

Table 4.3.2. Characteristics of HSSs and of analyzed geomagnetic storms

	1996	1997	1998	1999	2000	2001	2002	2003	2004	2005	2006	2007	2008
<b>Nr. HSS</b>	9	3	6	8	7	2	10	14	8	9	4	4	3
<b>VMax &gt;600km/s</b>	7	-	3	4	2	1	7	10	4	8	3	3	2
<b>DVmax &gt;300km/s</b>	1	-	-	4	-	1	6	5	2	7	3	3	2
<b>Dst&lt; -100</b>	1	-	1	-	-	-	4	1	-	1	-	-	-
<b>SSC</b>	1	2	2	7	1	2	2	-	3	3	1	2	2

Even if at maximum activity CH are limited (with some exceptions) to high latitudes zones, their compact structure determines the occurrence of some HSS that during their

propagation towards Earth can reach heliospherical latitudes such that they perturb the terrestrial magnetosphere. In these periods, the maximum speed of the HSS as well as the speed gradient reach higher values and geomagnetic perturbations can be induced. This is the situation for the years 1999, 2002 – 2003 (third and fourth row in Table 4.3.2). 2001, which belongs to the maximum activity phase of the SC 23, shows an unexpected low number of HSS. Considering the sunspot relative numbers, monthly mean values, this year shows a decrease between 2000 and 2002, years of maximum activity of SC23 (Fig. 16).

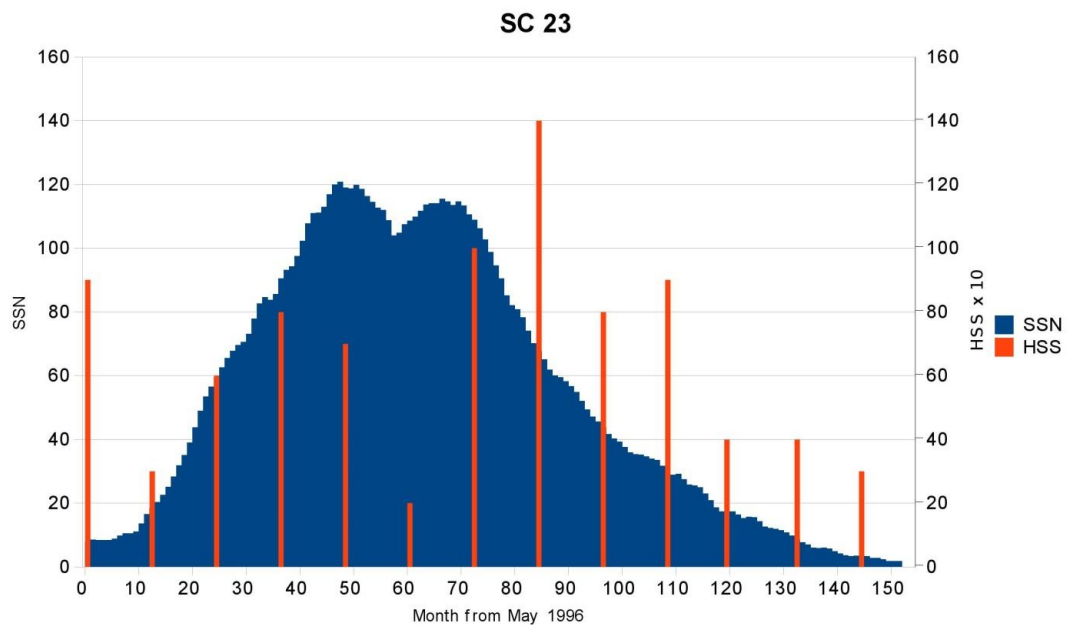


Fig. 16. SC 23 as seen in the smoothed monthly mean values (SSN) (blue).

Superimposed are histograms of annual values of HSS that have produced geomagnetic storms (red)

Even if at maximum activity CH are limited (with some exceptions) to high latitudes zones, their compact structure determines the occurrence of some HSS that during their propagation towards Earth can reach heliospherical latitudes such that they perturb the terrestrial magnetosphere. In these periods, the maximum speed of the HSS as well as the speed gradient reach higher values and geomagnetic perturbations can be induced. This is the situation for the years 1999, 2002 – 2003 (third and fourth row in Table 4.3.2). 2001, which belongs to the maximum activity phase of the SC 23, shows an unexpected low number of HSS. Considering the sunspot relative numbers, monthly mean values, this year shows a decrease between 2000 and 2002, years of maximum activity of SC23 (Fig. 16).

From the heliographic CH distribution analysis, we can conclude the following aspects essential for HSS geo-effectiveness:

- HSS triggered by CH found in the eastern hemisphere of the Sun do not perturb the terrestrial magnetosphere (because of the spiral propagation of the solar particles);
- CH position close to the central meridian ( $\pm 10^\circ$ ) of the solar disk, assures a geo-effectiveness of the HSS close to 60%;
- CH found in the western hemisphere, produced HSS with a geo-effectiveness up to 98%;
- The compact structure and extended surface of the CH contributes to the HSS energy, that can increase geo-effectiveness.
- CH position close to the central meridian ( $\pm 10^\circ$ ) of the solar disk, assures a geo-effectiveness of the HSS close to 60%;
- CH found in the western hemisphere, produced HSS with a geo-effectiveness up to 98%;
- The compact structure and extended surface of the CH contributes to the HSS energy, that can increase geo-effectiveness.

The annual distribution of **geomagnetic storms (GS)** starting with those of medium intensity for SC 23 is shown in Fig. 17. 2003 is noticed as a maximum for GS of medium intensity, 2002 for intense GS . In Table 4.3.2, the second last row shows the same year, 2002, for intense storms produced by HSS.

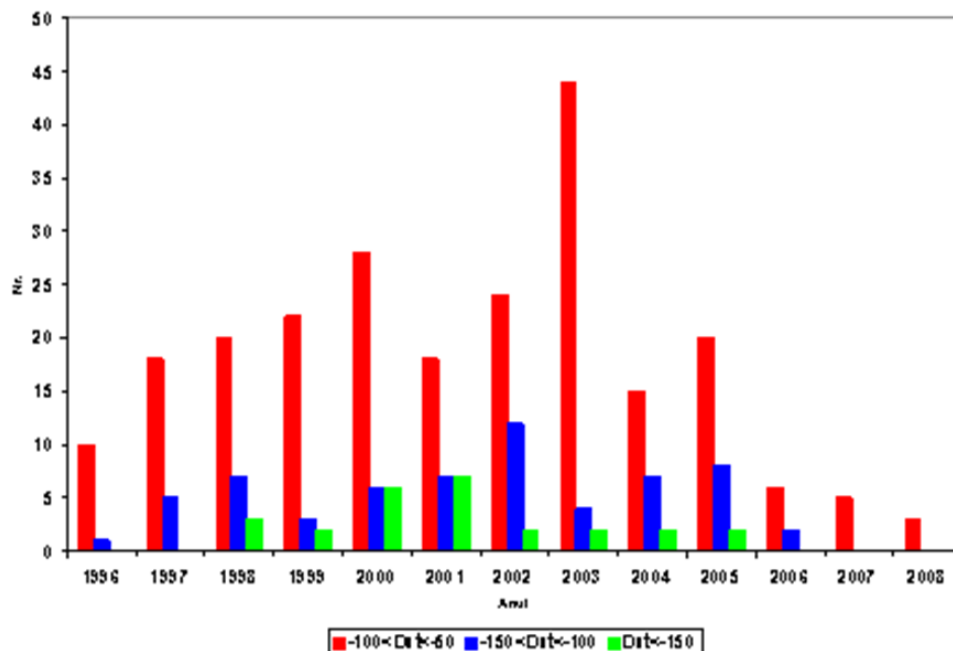


Fig. 17. Annual distribution of geomagnetic storms in SC23 by their intensity

(Maris & Maris, 2010, Complex Catalogue: GSs-HSSs, 1996 – 2008; available at:

[http://www.space-science.ro/new1/GS\\_HSS\\_Catalogue.html](http://www.space-science.ro/new1/GS_HSS_Catalogue.html))

The beginning of the storm structure shows the existence of a shock wave for those storms that have a sudden commencement (SSC). The maximum recorded in 1999, is due to the complex magnetic structure from the solar corona in the maximum phase, when the active regions extensions (by coronal mass ejections for example), favours the shock wave occurrence that propagates close to the Earth.

The energy transfer from the HSS to the terrestrial magnetosphere is produced by reconnection between the terrestrial magnetic field and the heliospheric magnetic field (HMF or IMF), that occur in front of the magnetosphere when the z direction component of the interplanetary magnetic field (Bz) in GSM coordinates, is negative.

From Table 4.3.1, from the data concerning Dst min, Bz values and the interval that maintains the Bz values negative before and close to the moment that Dst reaches its minimum values, we can infer:

- The interval between Bz min and Dst min is 1 – 3 hours, with few exceptions, when it lasts 4 or even 5 hours;
- Bz is negative throughout more hours, over 5, in most cases (90%), which provides an efficient energy transfer in magnetosphere, especially in the main phase of the GS (from the beginning to the Dst minimum moment);
- Just 8 % of GS are intense and these are different by the fact that Bz remains negative for longer periods (> 8 hours);
- By analysing Bz variability and comparing it to HSS parameters (Vmax and DVMax), we conclude that negative Bz insures greater geoefficiency of the HSS than the velocity (energy) of its particles.

Following this study, it is clear that:

- Observing CH can give clues to a possible geoeffective HSS by 3 – 4 days in advance;
- Recording a solar plasma increase in speed (a HSS) at ACE (Lagrangian point L1, 1.500.000 km in front of the magnetosphere) and along with Bz values analysis, makes a GS prognosis possible by at least 2 hours ahead its triggering.

## Chapter V. Dissemination of results

In the report period five papers have been published, as follows:

- Dobrica V., Demetrescu C., Greculeasa R., Isac A., 2012, On the crustal bias of repeat stations in Romania, *Annals of Geophysics*, 55, 6, 1145-1154, doi: 10.4401/ag-5442, Impact Factor ISI = 0.8.
- Dobrica V., Demetrescu C., Maris G., 2012, Solar wind dynamic pressure and magnetopause stand-off distance before the instrumental era, *Sun and Geosphere*, 7, 45-48.
- Dobrica V., Demetrescu C., Stefan C., 2013, Toward a better representation of the secular variation. Case study: the European network of geomagnetic observatories, *Earth, Planets, Space*, 65, 767–779, doi:10.5047/eps.2012.12.001, Impact Factor ISI = 2,921.
- Stefan C., Dobrica V., Demetrescu C., 2013, On the evolution of geomagnetic activity in the last 300 years. Implications regarding solar wind dynamic pressure and magnetopause standoff distance, *Sun and Geosphere*, 8(1), 7-10.
- Greculeasa R. A., Dobrica V., Demetrescu C., 2013, Sources of Geomagnetic Activity at Mid-Latitudes: Case Study – European Observatories, *Sun and Geosphere*, 8(1), 11-14.

Also, in 2012 and 2013 the team members of the contract participated to international scientific meetings (7 in 2012, 5 in 2013) with papers (16 in 2012, out of which 2 invited, 15 in 2013) and at 2 national scientific meetings (4 papers in 2012). The paper „Long-term external effects in annual means from observatory and main field models”, authors: Stefan C., Demetrescu C., Dobrica V., received the prize *Outstanding young scientist poster* at the General Assembly of EGU (European Geosciences Union) 2013.

We also mention in this section of the report that the web page of the project, <http://www.geodin.ro/IDEI2011/eng/index.html>, has been updated.

Project Director,

**Dr.Crișan Demetrescu**

Corresponding Member of the Romanian Academy